第34卷第11期 焊 接 学 报 Vol. 34 No. 11
2013年11月 TRANSACTIONS OF THE CHINA WELDING INSTITUTION November 2013

基于固有应变法预测双丝 CO_2 气体保护焊液压支架顶梁变形

方臣富， 吴文烈， 刘 川， 钟绪浪
(江苏科技大学 先进焊接技术省级重点实验室，镇江 212003)

方臣富

摘 要： 采用双丝 CO_2 气体保护焊方法焊接 30 mm 厚 Q690D 钢板全尺寸液压支架顶梁. 基于温度热源和热弹塑性算法对局部顶梁结构焊接变形进行计算，获得焊接固有应变，然后将固有应变施加在全尺寸壳单元顶梁模型上进行弹性计算，最终得到液压支架顶梁结构的焊接变形. 结果表明，结合小结构模型的热弹塑性法和大结构固有应变法，能高效预测大型结构的焊接变形且能保证一定精度，预测的液压支架顶梁焊接变形结果与试验结果符合较好；液压支架顶梁的焊接变形主要为角变形，且两侧分布不对称.

关键词： 液压支架；有限元；固有应变法；数值模拟；焊接变形
中图分类号： TG404 **文献标识码：** A **文章编号：** 0253－360X(2013)11－0001－04

0 序 言

液压支架是煤矿综采工作的关键设备，其中顶梁为箱体式厚壁大型焊接结构，焊接工作量非常大. 为了提高焊接生产效率，采用双丝 CO_2 气体保护焊焊接顶梁底板和筋板[1]. 但是液压支架顶梁和筋板焊缝长，整个结构经多道焊接后会变形，从而影响该结构后续工序安装和制造. 因此有必要对该类大型工程结构的焊接变形进行准确预测以便为调控变形提供理论依据. 虽然有限元数值模拟是预测焊接结构应力变形的有效方法，但焊接应力变形有限元模拟是高度非线性热力耦合计算，非常耗时. 大型工程结构的焊接应力变形数值模拟效率低下，严重阻碍了数值模拟在实际焊接工程中的应用发展.

国内外学者提出降维法[2]、子结构法[3]、固有应变法[4,5]、带状热源[6]等多种方法提高焊接应力变形的数值计算效率. 工程领域的大型结构焊接应力变形预测需要兼顾效率和精度. 固有应变法是具有较高精度的一种高效数值模拟方法. 获得准确反映焊接过程的固有应变是该方法的基础. Deng 等人[7]基于局部结构热弹塑性计算的固有变形来获得固有应变，将热弹塑性计算的高精度和固有应变法的高效率相结合，兼顾了计算精度和效率. 但小结构热弹塑性计算也需要足够大的模型尺寸以及细化网格才能保证最终获得的固有应变更准确反映实际焊接过程的应变，因此采用小结构热弹塑性有限元数值计算获取固有应变时也需要考虑高效计算.

文中采用高效的带状温度热源模型[8]提高焊接热弹塑性计算效率，针对 30 mm 厚 Q690D 钢板全尺寸液压支架顶梁双丝 CO_2 气体保护焊焊接变形，首先进行小结构三维热弹塑性分析获得焊接固有应变，然后将固有应变施加在全尺寸壳单元模型上进行弹性计算，最终获得液压梁支架顶梁结构的焊接变形.

1 试验方法

焊接试验的母材为 Q690D 钢，填充材料为直径 1.2 mm 的 MK·GHS80 实芯焊丝，保护气体为 80% Ar + 20% CO_2 富氩混合气体. 顶梁结构的底板和筋板经焊接后尺寸如图 1 所示.

每块筋板和底板的焊接采用 4 台 OTC XD 600G 焊接电源同时进行 GMAW 双丝焊，如图 2 所示，共进行 3 道焊接，焊缝形貌如图 3 所示. 该结构总焊接长度达到 67.2 m. 焊接结束后将焊接件翻转采用 CIMCORE MODEL 5126 三坐标测量仪测试底板的变形.

收稿日期：2013－05－21
基金项目：国家自然科学基金资助项目(51275224)；江苏科技大学博士科研启动基金资助项目(35061107)

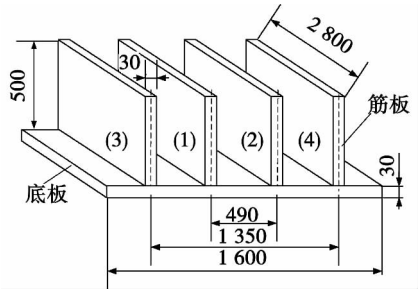

图 1 焊接结构尺寸(mm)

Fig. 1 Dimensions of welded structure

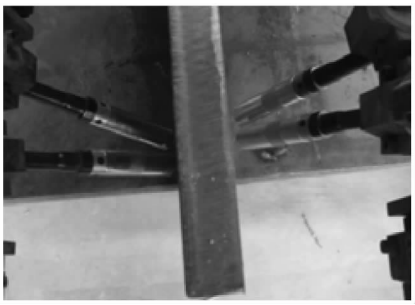

图 2 双丝焊接

Fig. 2 Twin-wire welding

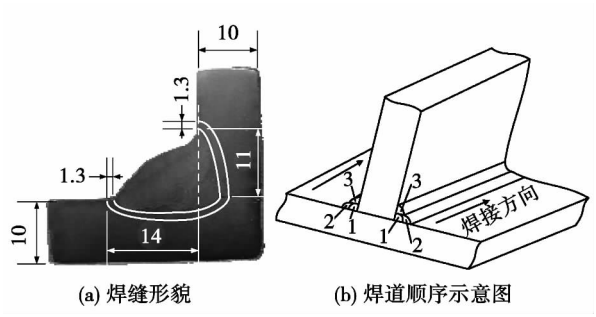

图 3 焊缝形貌和焊道顺序示意图(mm)

Fig. 3 Schematic diagram of weld profile and welding passes

2 计算过程和计算模型

从液压支架顶梁结构中选取小结构,尺寸如图 4 所示.

该小结构的焊接方法、坡口形式、焊道顺序等与液压支架结构一致. 首先以该小结构为对象进行三维热弹塑性有限元计算,然后根据计算结果获得该类结构和焊接方法的横向收缩、纵向收缩及角变形,并将这 3 个量转换为横向固有应变和纵向固有应变;最后建立与液压支架结构尺寸一致的壳单元模型,将固有应变施加在该壳单元模型上的焊缝区域进行弹性计算获得焊接变形.

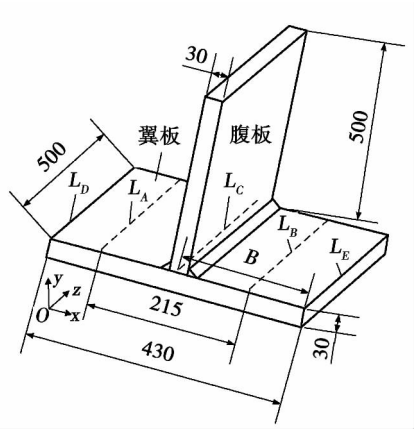

图 4 小结构尺寸示意图(mm)

Fig. 4 Dimensions of small structure

2.1 热弹塑性计算模型和计算过程

热弹塑性计算模型的焊缝区域有限元网格如图 5 所示,该模型中焊缝尺寸与图 3 中实际焊缝一致,各焊道填充金属面积进行适当简化,焊缝区域的单元尺寸约为 10 mm × 2 mm × 2 mm. 首先采用高效的温度热源计算焊接瞬态温度场,利用生死单元技术实现焊缝金属随焊接生长过程;然后将瞬态温度场结果作为负载获得该小结构的焊接变形. 计算用随温度变化的力学性能来自文献[9,10].

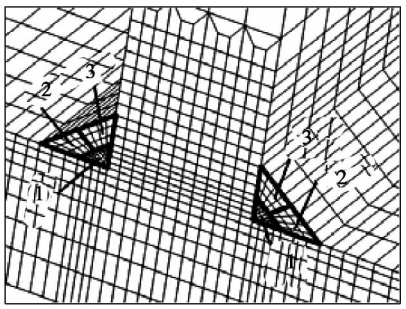

图 5 焊缝区域有限元网格

Fig. 5 Weld zone mesh of small structure

2.2 固有变形和固有应变

通过小结构模型计算的变形结果获得纵向收缩、横向收缩和角变形,然后计算横向和纵向固有应变. 根据文献[7],纵向收缩量 F 可采用下式计算,即

$$F = \int E\varepsilon_{\mathrm{L}}^{\mathrm{p}}\mathrm{d}A \tag{1}$$

式中: E 为弹性模量; $\varepsilon_{\mathrm{L}}^{\mathrm{p}}$ 为小模型计算得到的中截面上焊接方向(纵向)的塑性应变; A 为中截面位置的横截面面积.

横向收缩量 S 由下式进行计算,即

$$S = U_{yA} - U_{yB} \tag{2}$$

式中：U_{yA}，U_{yB}为图 4 中计算得到的 L_A 和 L_B 线（翼板中线）横向位移.

角变形量 β 可计算为

$$\beta = \left[\arcsin\left(\frac{U_{yD}-U_{yC}}{B}\right)+\arcsin\left(\frac{U_{yE}-U_{yC}}{B}\right)\right]/2 \tag{3}$$

式中：B 为腹板的半宽；U_{yC}，U_{yD}，U_{yE}分别为图 4 中线 L_C，L_D，L_E 的 y 向位移.

根据式（1），式（2）和式（3）得到的 F，S 和 β，可以得到腹板和翼板的纵向固有应变 $\varepsilon^*_{\mathrm{Lf}}$，$\varepsilon^*_{\mathrm{Lw}}$为

$$\varepsilon^*_{\mathrm{Lf}} = -\frac{FQ_{\mathrm{f}}}{2B_{\mathrm{f}}h_{\mathrm{f}}EQ_{\mathrm{t}}} \tag{4}$$

$$\varepsilon^*_{\mathrm{Lw}} = -\frac{FQ_{\mathrm{w}}}{H_{\mathrm{w}}h_{\mathrm{w}}EQ_{\mathrm{t}}} \tag{5}$$

式中：h_{w} 和 h_{f} 为翼板和腹板的厚度；B_{f} 和 H_{w} 为腹板和翼板上热弹塑性计算得到的塑性应变分布宽度；Q_{t} 为 3 道焊接热输入的总和；Q_{f}，Q_{w} 分别为腹板和翼板的热输入，文中翼板的热输入占总热输入的 2/3，而腹板热输入为总热输入的 1/3.

不考虑腹板上的横向固有应变，根据 Luo 等人[8]的研究，翼板上固有应变施加区域为两层壳单元，每层的横向固有应变 $\varepsilon^{1*}_{\mathrm{T}}$ 和 $\varepsilon^{2*}_{\mathrm{T}}$ 按照下式计算，即

$$\varepsilon^{1*}_{\mathrm{T}} = \left(S-\frac{2}{3}h_{\mathrm{f}}\beta\right)/B_{\mathrm{f}} \tag{6}$$

$$\varepsilon^{2*}_{\mathrm{T}} = \left(S+\frac{2}{3}h_{\mathrm{f}}\beta\right)/B_{\mathrm{f}} \tag{7}$$

3　计算结果

3.1　弹塑性计算结果

通过热弹塑性方法计算得到的小结构 y 向焊接变形（角变形）如图 6 所示（变形量放大 50 倍）. 从图 6 中看出，该小模型经 3 道双丝对称焊接后，其 y 向变形主要发生在翼板上，且两侧完全对称.

3.2　液压支架顶梁焊接变形

将小结构热弹塑性方法计算得到的横向和纵向固有应变施加在液压支架全尺寸壳单元模型上，经弹性计算得到的 y 向变形量如图 7 所示（变形量放大 20 倍）.

从图 7 中看出，整个液压支架顶梁的焊接变形主要为底板的角变形（即 y 向变形）；该结构底板一侧 y 向变形量达到了约 10 mm，另一侧 y 向变形量约为 6 mm；这说明该液压支架的变形两侧不对称，这可能与施焊顺序和拘束位置相关；也可看出该结构底板沿纵向的变形较均匀. 该液压支架顶梁的总焊接长度达到 67.2 m，采用固有应变方法能高效获得该类大型结构的焊接变形.

3.3　试验验证

选取底板背面中部位置及侧边位置线（图 8a 所示），比较固有应变法计算和试验测试结果如图 8b 和图 8c 所示.

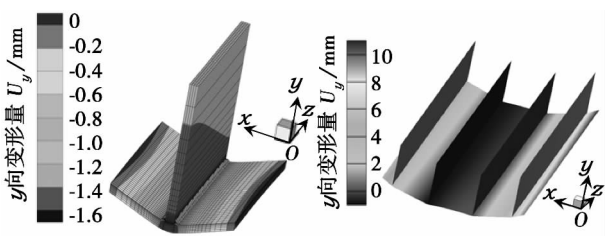

图 6　小结构焊接变形

Fig. 6　Residual distortion

图 7　顶梁焊接变形

Fig. 7　*y*-direction distortion

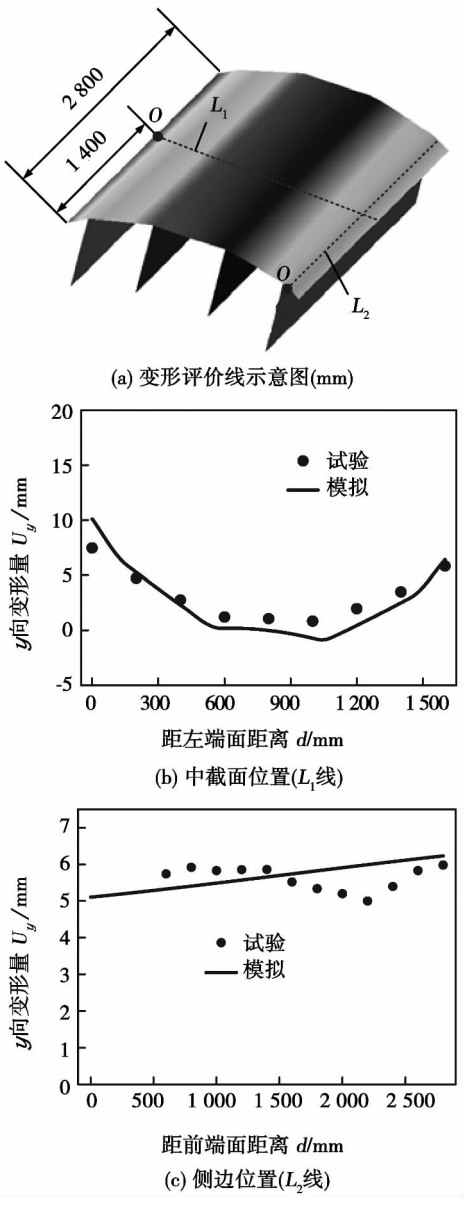

图 8　计算和试验测试结果比较

Fig. 8　Comparison between simulated and experimental distortion on base plate

从图 8b 中看出，液压支架顶梁底板中截面位置的计算焊接变形和试验测试结果符合较好，整个底板的 y 向变形(角变形)呈不对称分布，两侧的变形大，中间筋板位置的变形几乎为零. 图 8c 看出，距边缘 20 mm 位置的侧边线变形在纵向方向上的变化幅度较小，前后端变形量差距约 1 mm，说明该结构纵向的刚度大，焊缝的纵向收缩造成的变形较小. 测试的纵向变形局部位置呈现波浪变形，这可能是测试设备的测量臂短而造成侧边线测试基准变化所致，也可能是底板焊前局部存在波浪变形所致. 总体而言侧边位置的计算和试验测试结果的变形趋势接近.

4 结 论

(1) 基于小结构热弹塑性计算获得固有应变，然后将固有应变加载在大型焊接结构壳单元模型上弹性计算焊接变形，该方法能兼顾计算效率和精度，能够高效计算总焊接长度达 67.2 m 的大型结构焊接变形.

(2) 液压支架顶梁结构双丝多道 CO_2 气体保护焊的焊接变形以底板的角变形为主，最大变形量达到 10 mm，且两侧角变形呈不对称分布; 沿纵向的变形较均匀，前后端差距约 1 mm.

参考文献:

[1] Fang Chenfu, Meng Xiaohui, Hu Qingxian, *et al*. TANDEM and GMAW twin wire welding of Q690 steel used in hydraulic support [J]. Journal of Iron and Steel Research, 2012, 19(5): 79 - 85.

[2] Jiang Wei, Yahiaoui K, Laoui T, *et al*. Finite element simulation of multipass welding: full three-dimensional versus generalized plane strain or axisymmetric models [J]. The Journal of Strain Analysis for Engineering Design, 2005, 40(6): 587 - 597.

[3] 刘 川，张建勋. 基于动态子结构的三维焊接残余应力变形数值模拟 [J]. 焊接学报，2008，29(4)：21 - 24.
Liu Chuan, Zhang Jianxun. Numerical simulation of welding stresses and distortions based on 3D dynamic substructure method [J]. Transactions of the China Welding Institution, 2008, 29(4): 21 - 24.

[4] Luo Yu, Ishiyama M, Murakawa H. Welding deformation of plated with longitudinal curvature [J]. Transactions of Japan Welding Reasearch Institute, 1999, 28(2): 57 - 65.

[5] 汪建华，陆 皓，魏良武. 固有应变有限元法预测焊接变形理论及其应用 [J]. 焊接学报，2002，23(6)：36 - 40.
Wang Jianhua, Lu Hao, Wei Liangwu. Prediction of welding distortions based on theory of inherent strain by FEM and its application [J]. Transactions of the China Welding Institution, 2002, 23(6): 36 - 40.

[6] 蔡志鹏. 大型结构焊接变形数值计算的研究与应用 [D]. 北京：清华大学，2001.

[7] Deng Dean, Murakawa H, Liang Wei. Numerical simulation of welding distortion in large structures [J]. Computer Methods in Applied Mechanics and Engineering, 2007, 196(45/48): 4613 - 4627.

[8] 方臣富，王海松，刘 川，等. 缆式焊丝 CO_2 气体保护焊接头残余应力高效数值计算和试验 [J]. 焊接学报，2012，33(5)：17 - 20.
Fang Chenfu, Wang Haisong, Liu Chuan, *et al*. Efficient numerical simulation and experimental study on residual stress induced by GMAW with cable-type wire [J]. Transactions of the China Welding Institution, 2012, 33(5): 17 - 20.

[9] Chen Ju, Ben Young, Brian U. Behavior of high strength structural steel at elevated temperatures [J]. Journal of Structure Engineering, 2006, 132(12): 1948 - 1954.

[10] Chen Ju, Ben Young. Design of high strength structural steel columns at elevated temperatures [J]. Journal of Constructional Steel Research, 2008, 64(6): 689 - 703.

作者简介: 方臣富，男，1954 年出生，博士，教授，博士研究生导师. 主要从事焊接设备及工艺、焊接电弧物理的研究工作. 发表论文 50 余篇. Email: hjfangchenfu@yahoo.com.cn

通讯作者: 刘 川，男，博士，副教授. Email: chuanliu2003@126.com

MAIN TOPICS, ABSTRACTS & KEY WORDS

Welding deformation of top beam structure in hydraulic support by CO_2 double-wire gas shield welding based on inherent strain method FANG Chenfu, WU Wenlie, LIU Chuan, ZHONG Xulang (Provincial Key Laboratory of Advanced Welding Technology, Jiangsu University of Science and Technology, Zhenjiang 212003, China). pp 1 - 4

Abstract: The welding experiment on 30 mm thick Q690 steel plate in full-scale top beam structure of hydraulic support was carried out. The welding deformation of a relatively small structure selected from the top beam structure was firstly simulated with the thermal-elastic-plastic finite element method based on the efficient heat source model, and then the inherent strain was obtained from the small model, finally the acquired inherent strain was input into the full-scale shell element model of the hydraulic beam support structure to calculate the welding distortion deformation. The results show that, the proposed method can predict the welding deformations of large structures efficiently and accurately, the computational welding deformations of the top beam structure agree well with the experimental results; the angular distortion deformation is the main deformation of the top beam structure, which is not uniform on both sides.

Key words: hydraulic support; finite element method; inherent strain; numerical simulation; welding deformation

Analysis of 3D reconstruction algorithm of laser welding molten pool image GAO Xiangdong, YANG Yongchen, ZHANG Yanxi (School of Electromechanical Engineering, Guangdong University of Technology, Guangzhou 510006, China). pp 5 - 8

Abstract: The molten pool in high-power disk laser welding is related to the welding quality. The welding molten pool images were captured by a laser welding monitoring system. In order to reconstruct 3D shapes of the welding molten pools and further analyze the relationship between the shape features such as weld bead height, weld bead width and the welding quality, the shape from shading (SFS) technology based on single welding molten pool image was researched. 3D molten pool shapes could be recovered by the gray variations of welding molten pool image. The experimental apparatus included an auxiliary diode illuminant and a high-speed camera with near infrared filter to capture the welding molten pools in real time. The slant and tilt of illuminant source were estimated by the statistical algorithm. The 3D shape of welding molten pool surface was reconstructed by using the localization method of SFS. Also, the methods of median filter and cubic spline interpolation were applied to remove the noise and smooth the shape of molten pool. Experimental results showed that the proposed method can reconstruct the welding molten pool surface effectively. The 3D molten pool shape can be estimated by the molten pool image during high-power disk laser welding.

Key words: high-power disk laser welding; welding molten pool; 3D reconstruction

Effect of rotation frequency on microstructure and mechanical properties of refill friction spot welded Mg/Al dissimilar metals GUO Lijie[1], FENG Xiaosong[1], MIAO Yugang[2], HAN Duanfeng[2] (1. Shanghai Aerospace Equipments Manufacturer, Shanghai 200245, China; 2. College of Shipbuilding Engineering, Harbin Engineering University, Harbin 150001, China). pp 9 - 12

Abstract: AZ31 Mg alloy and 5A06 Al alloy were welded successfully with refill friction spot welding process. The shear stress of the spot joint with different tool rotation frequencies was tested. The effect of rotation frequency on the cross-section, interface layer and element distribution was analyzed. With the increase of the tool rotation speed, the shear stress of the joints increases firstly and then decreases. In particular, when the rotation speed is 2 400 r/min, the average shear stress can reach a maximum of 1.9 kN. When the rotation frequency is lower, the interface layer of Mg/Al is thiner. Due to the insufficient interface reaction, the phenomenon of incomplete fusion appears. If the rotation frequency is higher, the interface layer of Mg/Al is thicker (about 5 μm). The interface bonding is very good.

Key words: refill friction spot welding; dissimilar metals; rotation frequency; interface layer; mechanical properties

Formability and microstructure of magnesium alloy welded by A-TIG under magnetic field SU Yunhai[1,2], LIN Jinliang[1], JIANG Huanwen[1], LIU Zhengjun[1] (1. Liaoning Provincal Key Laboratory of Advaced Welding Technology and Automation, Shenyang Unviersity of Technology, Shenyang 110870, China; 2. Chinese National Engineering Research Center, Liaoning Julong Financial Equipment Corp., Anshan 114041, China). pp 13 - 16

Abstract: The AZ31B magnesium alloy plates of 5 mm in thickness were welded by A-TIG welding under longitudinal magnetic field. The mixed oxides were used as activating fluxes. The form factor, microstructure and mechanical properties of welded joint at different magnetic field parameters were tested. The effects of magnetic field parameters on A-TIG welding process of magnesium alloy were also investigated. The results show that the formability and microstructure of magnesium alloy welded joint can be improved due to the magnetic field. When the magnetic frequency is 10Hz and the magnetic current is 2 A, the form factor and properties of welded joint are tested, the form factor is 2.304 and the hardness is 980.98 MPa. The flow of molten pool will be changed by the activating fluxes and electromagnetic (which forming by magnetic field). The liquid metal in molten pool will move from all around to center, which makes the weld be deeper, refines the microstructure and improves the properties